



HAL
open science

An iterative subspace denoising algorithm for removing electroencephalogram ocular artifacts

Reza Sameni, Cedric Gouy-Pailler

► **To cite this version:**

Reza Sameni, Cedric Gouy-Pailler. An iterative subspace denoising algorithm for removing electroencephalogram ocular artifacts. *Journal of Neuroscience Methods*, 2014, 225, pp.97 - 105. 10.1016/j.jneumeth.2014.01.024 . hal-01863321

HAL Id: hal-01863321

<https://hal.science/hal-01863321>

Submitted on 22 Jun 2023

HAL is a multi-disciplinary open access archive for the deposit and dissemination of scientific research documents, whether they are published or not. The documents may come from teaching and research institutions in France or abroad, or from public or private research centers.

L'archive ouverte pluridisciplinaire **HAL**, est destinée au dépôt et à la diffusion de documents scientifiques de niveau recherche, publiés ou non, émanant des établissements d'enseignement et de recherche français ou étrangers, des laboratoires publics ou privés.

An Iterative Subspace Denoising Algorithm for Removing Electroencephalogram Ocular Artifacts

Reza Sameni* and Cédric Gouy-Pailler

R. Sameni is with the School of Electrical & Computer Engineering, Shiraz University, Shiraz, Iran, E-mail: rsameni@shirazu.ac.ir, Phone: +98 711 6133169, Fax: +98 711 6474605.

Cédric Gouy-Pailler is with Commissariat à l'Énergie Atomique et aux Énergies Alternatives – CEA, LIST, Laboratoire d'Analyse des Données et Intelligence des Systèmes, 91 191 Gif-sur-Yvette, CEDEX, France, E-mail: cedric.gouy-pailler@cea.fr, Phone: +33 169 088 147, Fax: +33 169 086 030.

Abstract

Background: Electroencephalogram (EEG) measurements are always contaminated by non-cerebral signals, which disturb EEG interpretability. Among the different artifacts, ocular artifacts are the most disturbing ones. In previous studies, limited improvement has been obtained using frequency-based methods. Spatial decomposition methods have shown to be more effective for removing ocular artifacts from EEG recordings. Nevertheless, these methods are not able to completely separate cerebral and ocular signals and commonly eliminate important features of the EEG.

New Method: In a previous study we have shown the applicability of a deflation algorithm based on generalized eigenvalue decomposition for separating desired and undesired signal subspaces. In this work, we extend this idea for the automatic detection and removal of electrooculogram (EOG) artifacts from multichannel EEG recordings. The notion of *effective number of identifiable dimensions*, is also used to estimate the number of dominant dimensions of the ocular subspace, which enables the precise and fast convergence of the algorithm.

Results: The method is applied on real and synthetic data. It is shown that the method enables the separation of cerebral and ocular signals with minimal interference with cerebral signals.

Comparison with Existing Method(s): The proposed approach is compared with two widely used denoising techniques based on independent component analysis (ICA).

Conclusions: It is shown that the algorithm outperformed ICA-based approaches. Moreover, the method is computationally efficient and is implemented in real-time. Due to its semi-automatic structure and low computational cost, it has broad applications in real-time EEG monitoring systems and brain-computer interface experiments.

Keywords: Subspace decomposition; Electroencephalogram denoising; Ocular artifacts; Semi-blind source separation

1. Introduction

Electroencephalography (EEG) is widely used for analyzing and interpreting human cerebral activity. EEG signals are usually interpreted by means of spectral and topographical measures that reflect global activity of the brain network. However, EEG measurements are always contaminated by non-cerebral signals, which may disturb the interpretation of the brain activity. This issue has become a recurrent problem, for example in brain-computer interface (BCI), where it has been proved to decrease the classification rates of mental tasks inferred from the EEG (Thulasidas et al., 2004). Among the commonly encountered artifacts, ocular artifacts are considered as the most disturbing ones.

Ocular artifacts generally occur during blinking or saccades of the eye and are featured by high amplitude transient artifacts that defect the EEG. They are best recorded by an electrooculogram (EOG) electrode or a pair of electrodes located close to the eyes. The high amplitude peaks are not seen on all EEG channels; but mainly (and almost exclusively) on the frontoparietal and occipital electrodes. These peaks are considered as

one of the most considerable artifacts in EEG studies (Koles, 1991; Gratton et al., 1983; Gasser et al., 1992).

Various methods have been proposed to remove ocular artifacts from EEG recordings (cf. (Fatourechhi et al., 2007; Croft et al., 2005) for a survey). Limited improvement has been obtained using straightforward frequency-based methods such as linear time-invariant filtering. The rationale behind this approach is that ocular artifacts are mainly constrained to low frequencies, especially below 10 Hz. Linear spatial decomposition methods have also raised interest for removing EEG ocular artifacts. Due to the quasi-static approximation usually admitted in common EEG analysis, a linear approximation exists between electrical dipole sources and electrode measurements. Therefore, linear mixtures of the electrode measurements can be used to separate noise and signal subspaces. For example, principal components analysis (PCA) has led to relatively satisfying results. Nevertheless, it has been argued that PCA is not able to completely separate cerebral and ocular signals, due to their possible dependence (Fatourechhi et al., 2007). Therefore, removing the most contaminated principal components cannot

guarantee cerebral signals integrity.

Another common way of removing EOG artifacts from the EEG is to use subtraction-based approaches (Romero et al., 2008; He et al., 2004). Here, the idea is to use the clean EOG recordings to remove ocular signals from the EEG by a simple subtraction of a scaled version of the EOG. However, due to the bipolar nature of ocular artifacts, the signals contaminated over the EEG do not fully resemble the recorded EOG. Therefore, subtraction-based approaches have not been very effective. Moreover, there is no evidence that signals recorded from EOG leads are free of EEG. Thus by subtracting the EOG, one may also remove small portions of the background EEG.

More recently, a popular method for removing these artifacts is to apply independent component analysis (ICA) on multichannel EEG recordings and to remove the components that are highly correlated with a reference EOG channel (Jung et al., 2000; Ille et al., 2002; Barbati et al., 2004; Chan et al., 2010; Delorme et al., 2007; Flexer et al., 2005). What makes this method challenging, is that it is not always possible to associate the components extracted by ICA to the EOG in an automatic and unsupervised manner. Many works have been carried out to design efficient criteria based on the spatial topography of ocular artifacts to focus on the most probable contaminated components (Li et al., 2006; Ille et al., 2002; Hesse and James, 2006). Nevertheless, this approach has not drawn high interests in the BCI community. Moreover, EEG recordings can be rather noisy, and since ICA is based on a measure of independence (and not a measure of signal “cleanness”), the noise in the input channels can be even amplified by ICA, which again makes the detection of the true EOG component rather difficult. Lastly, most ICA methods are blind to Gaussian noise and spread the noise among the extracted components, which is undesired.

In recent studies we have shown the applicability of a deflation algorithm based on *generalized eigenvalue decomposition* (GEVD) for separating desired and undesired signal subspaces (Sameni et al., 2010a,b; Gouy-Pailler et al., 2009; Amini et al., 2008; Sameni et al., 2008). In these studies, one of the advantages of GEVD over other source separation techniques was the ability of ranking the extracted components in order of interest, which provided a means of automatic and unsupervised signal decomposition and filtering.

In this work, we extend this idea to the automatic detection and removal of EOG artifacts from multichannel EEG recordings. The recently developed notion of *effective number of identifiable dimensions* (Nadakuditi and Silverstein, 2010), is also used to estimate the number of dominant dimensions of the ocular subspace. This notion enables precise and fast convergence of the proposed algorithm.

The remainder of this paper is organized as follows: in Section 2 the proposed framework is presented; Section 3 addresses the problem of ocular subspace dimension estimation and its impact on the algorithm, the results of this method are presented in Section 4 over simulated and real signals. The last section is devoted to conclusion and perspectives.

2. Signal decomposition by deflation

2.1. A linear transform for EOG and EEG separation

We assume an array of n zero-mean¹ EEG channels denoted by $\mathbf{x}(t)$ and a reference EOG channel denoted by $r(t)$. Due to the spiky nature of the EOG, it is typically possible to detect (although approximately) the onset and offset times of the EOG artifacts from the reference EOG channel. For this, we define $p(t)$, the moving average of the EOG signal power within a sliding window of length w around t ,

$$p(t) \doteq \frac{1}{w} \sum_{\tau=-w/2}^{w/2} r(t-\tau)^2 \quad (1)$$

Using this definition, an EOG is detected whenever $p(t)$ exceeds some predefined threshold th . Accordingly, the *active epochs* of the EOG can be defined as follows

$$t_a \doteq \{t | p(t) \geq th\} \quad (2)$$

The procedure of finding the offsets and onsets of the EOG does not need to be perfect, and the results can be further improved in a recursive procedure.

As proposed in (Sameni et al., 2010b), we next seek linear transforms of the multichannel recordings $\mathbf{x}(t)$, that maximally resemble the EOG, in the sense that the power of the extracted signals are concentrated during the active time epochs. Denoting $y(t) = \mathbf{b}^T \mathbf{x}(t)$, where $\mathbf{b} \in \mathbb{R}^n$, the following cost function is maximized:

$$\zeta(\mathbf{b}) = \frac{\mathbb{E}_{t_a} \{y^2(t_a)\}}{\mathbb{E}_t \{y^2(t)\}} = \frac{\mathbf{b}^T \mathbb{E}_{t_a} \{\mathbf{x}(t_a)\mathbf{x}(t_a)^T\} \mathbf{b}}{\mathbf{b}^T \mathbb{E}_t \{\mathbf{x}(t)\mathbf{x}(t)^T\} \mathbf{b}} \quad (3)$$

where $\mathbb{E}_t\{\cdot\}$ and $\mathbb{E}_{t_a}\{\cdot\}$ represent averaging over t and t_a , respectively, and \mathbf{b} is the vector of coefficients to be found. The idea behind this cost function is to find linear mixtures of the input signals, with a maximal energy ratio during the EOG active time epochs, t_a . Equation (3) is in the form of the Rayleigh quotient (Strang, 1988), and its maximum is achieved by the joint diagonalization of two matrices (also known as GEVD):

$$\begin{cases} \mathbf{B}\mathbf{C}_x\mathbf{B}^T = \mathbf{I} \\ \mathbf{B}\mathbf{D}_x\mathbf{B}^T = \mathbf{\Lambda} \end{cases}, \quad (4)$$

where $\mathbf{\Lambda}$ is a diagonal matrix containing the generalized eigenvalues on its diagonal in descending order, $\mathbf{B} = [\mathbf{b}_1, \mathbf{b}_2, \dots, \mathbf{b}_n]$ is the matrix containing the generalized eigenvectors on its columns², \mathbf{C}_x is the covariance matrix of the EEG channels over the whole dataset, and \mathbf{D}_x is the covariance matrix of the data during the active periods of the EOG, respectively defined as

$$\mathbf{C}_x \doteq \mathbb{E}_t \{\mathbf{x}(t)\mathbf{x}(t)^T\}, \quad (5)$$

¹The zero-mean assumption avoids biased estimates of later defined covariance matrices. This assumption does not limit the generalization of the method.

²Note that, contrary to the eigenvalues of symmetric matrices that are mutually orthogonal, generalized eigenvectors, i.e., the columns of \mathbf{B} , are not generally orthogonal to one other; but following (4) they are “ \mathbf{C}_x -orthogonal” (Strang, 1988, p. 344).

$$\mathbf{D}_x \doteq \mathbb{E}_{t_a} \{\mathbf{x}(t_a)\mathbf{x}(t_a)^T\} . \quad (6)$$

As suggested in (Sameni et al., 2010b), the intuition behind this method is to achieve decorrelated components that are at the same time *globally* and *locally* decorrelated. Global decorrelation is achieved by diagonalizing (and sphering) \mathbf{C}_x , which assures that the later extracted components have no redundancy up to second order statistics. In addition, the diagonalization of \mathbf{D}_x assures that the achieved components are also locally decorrelated over the active EOG epochs.

The signals may now be decomposed as

$$\mathbf{y}(t) = \mathbf{B}^T \mathbf{x}(t) \quad (7)$$

where the elements of $\mathbf{y}(t)$ correspond to a linear transform of the original data $\mathbf{x}(t)$ ranked according to their resemblance with the EOG activation epochs. In other words, $y_1(t)$ mostly resembles the EOG, while $y_n(t)$ is the least resembling the EOG.

2.2. Signal vs. noise separation

Using (7), the components are ranked descendingly according to their resemblance with the EOG. The next step is to remove the ocular artifacts from the most contaminated components using a linear or nonlinear transformation. The result of this noise removal, denoted by $\mathbf{z}(t) \doteq (z_1(t), \dots, z_n(t))^T$, can be expressed as

$$z_i(t) = f_i[y_i(t)] \quad , \quad i = 1, \dots, n \quad (8)$$

The denoising transform must be carefully chosen to remove ocular artifacts from the most contaminated signals, while preserving the non-EOG components. The simplest approach is to nullify the first m ($m \ll n$) components of $\mathbf{y}(t)$. The preliminary results of this approach were presented in (Gouy-Pailler et al., 2009). This approach eliminates the effect of the EOG and EEG components within the first m channels. However, the rank of the multichannel signals is also reduced to $n - m$. A better approach, which is adopted here and preserves the rank of the signals and preserves the non-EOG components is to use an appropriate denoising scheme such as wavelet denoisers over the first m components of $\mathbf{y}(t)$. Next, the denoised signals $z_i(t)$ are back-projected to the original signal space using \mathbf{B}^{-T} , the inverse of the decomposing matrix.

2.3. Iterative decomposition

To this end, the most dominant EOG components are eliminated through a combination of a linear decomposition (projection), denoising, and recomposition (back-projection). The results can be further improved by repeating the upper mentioned method in a recursive procedure (Figure 1), each time re-estimating the EOG active times.

In order to re-estimate the onset and offsets of the EOG and its activation epochs in each iteration, one can define the vector $\mathbf{y}_m(t) \doteq [y_1(t), \dots, y_m(t)]^T$, which is a vector of the m components that most resemble the EOG. Now, the reference EOG signal used in (1) can be recalculated as follows

$$r(t) = \|\mathbf{y}_m(t)\| \quad (9)$$

where $\|\cdot\|$ represents the vector norm (2-norm or Frobenius norm). All the other steps of the algorithm are repeated in each iteration. In fact, by repeating this procedure in several iterations, a better estimate of the EOG will be achieved, which is of special interest for the cases that a good EOG reference is not available. Therefore, one can start with a coarse EOG onset and offset estimate and improve this estimate in later iterations. The iterative procedure is repeated until the residual signals satisfy some predefined criterion. Alternatively, the algorithm may be repeated for a number of fixed iterations.

This overall algorithm can be summarized as follows:

Iterative EOG Cancellation Algorithm:

- 1: $\mathbf{x}^{(0)}(t) \leftarrow \mathbf{x}(t)$, $k \leftarrow 0$
- 2: $r(t) \leftarrow$ reference EOG channel
- 3: **repeat**
- 4: $p(t) \leftarrow \frac{1}{w} \sum_{\tau=-w/2}^{w/2} r(t - \tau)^2$
- 5: $t_a \leftarrow \{t | p(t) \geq th\}$
- 6: $\mathbf{C}_x \leftarrow \mathbb{E}_t \{\mathbf{x}^{(k)}(t)\mathbf{x}^{(k)}(t)^T\}$
- 7: $\mathbf{D}_x \leftarrow \mathbb{E}_{t_a} \{\mathbf{x}^{(k)}(t_a)\mathbf{x}^{(k)}(t_a)^T\}$
- 8: $\mathbf{B} \leftarrow \text{GEVD}(\mathbf{D}_x, \mathbf{C}_x)$
- 9: $\mathbf{y}(t) \leftarrow \mathbf{B}^T \mathbf{x}^{(k)}(t)$
- 10: Estimate m : number of EOG dimensions
- 11: $\mathbf{z}(t) \leftarrow \mathbf{f}(\mathbf{y}(t), m)$
- 12: $\mathbf{x}^{(k+1)}(t) \leftarrow \mathbf{B}^{-T} \mathbf{z}(t)$
- 13: $\mathbf{y}_m(t) \leftarrow [y_1(t), \dots, y_m(t)]^T$
- 14: $r(t) \leftarrow \|\mathbf{y}_m(t)\|$
- 15: $k \leftarrow k + 1$
- 16: **until** $\Delta(\mathbf{x}^{(k)}(t)) \leq c$

In this algorithm, $\mathbf{f}(\cdot, m)$ is the denoising operator applied to the first m components of $\mathbf{y}(t)$, $\Delta(\cdot)$ is a measure of the EOG removal used as a stopping criterion and c is a predefined threshold, which are both rather subjective. For this application, we select

$$\Delta(\mathbf{x}^{(k)}(t)) \doteq \frac{\text{tr}(\sum_{t_a} \mathbf{x}^{(k)}(t_a)\mathbf{x}^{(k)}(t_a)^T)}{\text{tr}(\sum_t \mathbf{x}^{(k)}(t)\mathbf{x}^{(k)}(t)^T)} \quad (10)$$

where $\text{tr}(\cdot)$ denotes matrix trace and \sum_t and \sum_{t_a} denote summations over the indexes t and t_a , respectively. Since $N(t_a) \leq N(t)$ ³, by definition $0 \leq \Delta(\mathbf{x}^{(k)}(t)) \leq 1$, and the algorithm is expected to reduce $\Delta(\cdot)$ in successive iterations⁴. A similar index can be defined for each channel

$$\delta_i(\mathbf{x}^{(k)}(t)) \doteq \frac{\sum_{t_a} x_i^{(k)}(t_a)^2}{\sum_t x_i^{(k)}(t)^2} \quad (11)$$

where $x_i^{(k)}(t)$ is the i th channel of $\mathbf{x}^{(k)}(t)$. In (Sameni et al., 2010b), alternative measures were presented for pseudo-periodic signals.

2.4. Implementation issues

The proposed method can be implemented for real-time and automatic preprocessing of EEG measurements. In fact, since the noisy components are automatically extracted as the first

³ $N(\cdot)$ denotes the number of elements of a set.

⁴Ideally $\Delta(\cdot)$ approaches zero as k increases.

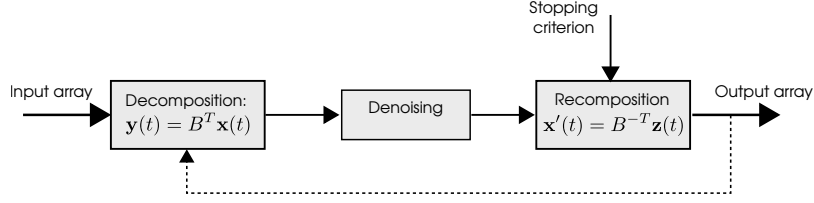


Figure 1: The iterative decomposition scheme adapted from (Sameni et al., 2010b).

components of GEVD, no supervision is required for removing these components. The window length for computing the time-varying EOG energy can be chosen according to the sampling frequency and the expected duration of a typical ocular blink (about 300ms).

The algorithm also requires the energy threshold th , to find the onsets and offsets of ocular artifacts given the EOG energy. Due to the iterative procedure, a first estimation of this threshold does not need to be perfect. It can either be set to a default value (e.g. 50% of the peak of instantaneous energy) for automatic denoising, or manually be chosen by visual inspection of short periods of typical datasets. In the results section, an alternative approach, with stronger theoretical support, based on a hypothesis test is proposed.

One of the limitations of the method is that enough data is needed for a consistent estimate of the covariance matrices, especially for the estimation of the covariance matrix during ocular activity (\mathbf{D}_x), where the number of samples used in the calculation of \mathbf{D}_x is much less than the total signal length. Therefore, depending on the sampling rate and data dimensions, appropriate robust covariance estimators may be used (cf. Rousseeuw and Leroy (2003) for a survey).

Finally, the number of GEVD components to denoise (m) and the denoising technique $\mathbf{f}(\cdot)$ should be chosen such as to eliminate the ocular artifacts and to preserve the EEG components. These factors also depend on the dimensionality of the data. For the proposed application $\mathbf{f}(\cdot)$ is a wavelet denoiser from the Daubechies least-asymmetric family (Nason, 2008). The selection of this mother wavelet was due to its temporal similarity with typical EOG and saccades which enables better EEG denoising. Although other denoising schemes are also applicable in the proposed deflation technique, wavelet denoising with a profound theoretical support has been extensively used for signal denoising in various applications. Specifically, for this application, the advantage of the wavelet denoising is that it can be applied to signals with minimal assumptions about their temporal shape (Donoho and Johnstone, 1995).

Finally, the dimensionality of the ocular signal subspace is studied in the following section, based on the recently presented notion of effective number of dimensions (Nadakuditi and Silvesterstein, 2010). Alternatively, one may choose fixed or empirical values for m , depending on the application.

3. Ocular subspace dimension estimation

It is known that ocular signals do not have a punctual origin. Instead, they are mainly spread throughout the frontal and oc-

cipital regions of the brain. This explains why classical ICA techniques are not always successful in separating ocular artifacts from the background EEG; since the punctuality assumption of sources is not met. This commonly results in the extraction of multiple signals that are correlated with the EOG, which appear as residual traces of ocular artifacts in the background EEG. Due to the distributedness of the ocular sources, the exact number of dimensions of the ocular subspace is unknown (and not necessarily finite). However, for the hereby proposed method and ICA-based techniques, it is helpful to calculate the number of dominant ocular signal dimensions, which can be used as the parameter m in the deflation denoising algorithm. The problem can be formally stated as follows. We assume

$$\mathbf{x}(t) = \mathbf{A}\mathbf{s}(t) + \mathbf{n}(t) \quad (12)$$

where $\mathbf{x}(t) \in \mathbb{R}^n$ ($t = 1, \dots, T$) is the zero-mean multichannel observation defined in section 2.1, $\mathbf{s}(t) \in \mathbb{R}^m$ is the ocular signal with an unknown dimension m ($m \leq n$), $\mathbf{A} \in \mathbb{R}^{n \times m}$ is a projector from the ocular subspace to the sensor subspace, and $\mathbf{n}(t) \in \mathbb{R}^n$ contains all the non-ocular components, including the EEG, background noise, etc. We further assume that $T > n$, which is a realistic assumption in our application and permits us to use simplified versions of dimension estimation algorithms. The T -sample estimate of the covariance matrix of $\mathbf{x}(t)$ is

$$\mathbf{R}_x = \sum_{t=1}^T \mathbf{x}(t)\mathbf{x}(t)^T \quad (13)$$

with eigenvalues $\lambda_1 \geq \lambda_2 \geq \dots \geq \lambda_n$. The objective is to find m , the number of dominant (or effective) ocular dimensions.

There are several classical methods for estimating the number of dimensions of a signal embedded in noise. In the following two of the methods, which have been used for this study and were proved to be more effective for EEG/EOG signals in our studies are further discussed.

3.1. Eigenvalue-based measure of dimensionality

We assume that the ocular ($\mathbf{s}(t)$) and non-ocular ($\mathbf{n}(t)$) signals be independent. Furthermore, we assume that the elements of the non-ocular signal $\mathbf{n}(t)$ are uncorrelated and have equal variances, i.e., $\mathbf{R}_n = \sigma^2 \mathbf{I}$ (the latter is only a simplifying assumption used for illustrating the idea and is not necessarily true in reality). Under these assumptions, the covariance matrix of the observations $\mathbf{x}(t)$ is

$$\mathbf{R}_x = \mathbf{A}\mathbf{R}_s\mathbf{A}^T + \sigma^2\mathbf{I} \quad (14)$$

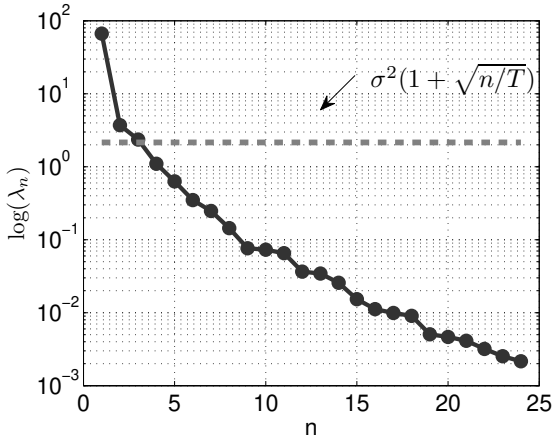


Figure 2: The logarithmic plot of the eigenvalues of \mathbf{R}_x for a typical segment of EEG data. The dashed line indicates the threshold for the effective number of identifiable signals, discussed in section 3.2. In this example three of the eigenvalues exceed this threshold.

Assuming that \mathbf{A} is full column rank, $\mathbf{A}\mathbf{R}_x\mathbf{A}^T$ is rank- m . Hence, the $n - m$ smallest eigenvalues of \mathbf{R}_x are equal to σ^2 . Therefore, under the mentioned assumptions, a simple approach to find m is to calculate and rank the eigenvalues of \mathbf{R}_x and to identify where the smallest eigenvalues are equal. However, for EEG/EOG signals, the non-ocular components (such as the EEG) have inter-correlations, their variances are not necessarily equal, and only an estimate of \mathbf{R}_x is available based on a finite number of samples, which make the method inapplicable for the problem of interest. In (Lee and Verleysen, 2007), other eigenvalue-based techniques have also been discussed. For instance, a considerable change in the slope of the ranked eigenvalue plots, or a change of slope in the logarithmic plot of the ranked eigenvalues, can also be interpreted as potential dimension changes. In Figure 2, the logarithmic plot of the sorted eigenvalues are depicted for a typical EEG signal of length 20s, recorded from 25 channels. It is observed that there is a change of slope between $m = 1$ and $m = 3$. It is however difficult to identify a precise value for m .

3.2. Information theoretical measures of dimensionality

To date, many information theoretical measures have been proposed for estimating the number of dimensions of a signal embedded in noise, including the Akaike information criteria (AIC) (van Trees, 2002; Nadakuditi and Edelman, 2008, Ch. 4), minimum descriptive length (MDL) criterion and a more recent measure proposed by Nadakuditi and Edelman (Nadakuditi and Edelman, 2008). However, as discussed in (Nadakuditi and Edelman, 2008) for high-dimensional noisy data with limited sample size, there is no clear-cut on the exact number of dimensions using information theoretical measures. Based on this fact, Nadakuditi and Edelman proposed the notion of *effective number of identifiable signals* for such data. They heuristically define the effective number of identifiable signals as “the number of signal eigenvalues of the population covariance matrix (here \mathbf{R}_x), which exceed the noise variance (σ^2) by a factor

strictly greater than $1 + \sqrt{n/T}$ ”, i.e.,

$$\hat{m}_{\text{eff}} = N(\{\lambda_i | \lambda_i > \sigma^2(1 + \sqrt{n/T}), i = 1, \dots, n\}) \quad (15)$$

where, as before, $N(\cdot)$ represents the number of elements of a set. In Figure 2, the horizontal line represents the threshold $\sigma^2(1 + \sqrt{n/T})$. We can see that for a sample EEG signal, the number of eigenvalues that exceed this threshold (the effective number of identifiable signals) is equal to $m = 3$.

In the hereby proposed algorithm, one can set the number of signals that are denoised in each iteration of the algorithm (m) smaller or equal to the effective number of identifiable signals calculated from (15). In fact, the selection of m is a compromise between accuracy and speed. By selecting $m = 1$ we only eliminate one of the ocular dimensions in each iteration of the deflation algorithm, which makes the algorithm rather conservative in removing ocular artifacts and requires more iterations to remove the entire ocular subspace. On the other hand, if $\hat{m}_{\text{eff}} > 1$, setting $m = \hat{m}_{\text{eff}}$ removes more ocular related components in each iteration, which makes the convergence faster; but has the risk of removing non-ocular components. In the following section, a real example is presented, which uses the idea of effective number of identifiable signals in the denoising algorithm.

4. Results

4.1. Simulated data

The performance of the proposed approach is assessed by means of a simulation study. First a surrogate method is employed to generate artificial, yet plausible, EEG recordings in a two-fold approach. On the one hand, artifact-free real EEG measurements serve as a basis to train a multivariate autoregressive p -order filter (Anderson et al., 1998) (in the following $p = 8$). In such a model, the current EEG observation is represented as the weighted sum of p previous observations

$$\mathbf{EEG}(t) = - \sum_{i=1}^p A_i \mathbf{EEG}(t-i) + \varepsilon(t), \quad (16)$$

in which $A_i \in \mathbb{R}^{n \times n}$ ($i = 1, \dots, p$) and ε represents the zero-mean error of the model. While the model is trained using generalized Levinson’s recursions, a straightforward way to generate new artifact-free EEG signals consists in injecting random Gaussian noise to the previously trained recursive model (16). Although a univariate autoregressive approach would have been sufficient to render temporal dependencies inside single channel EEG signals, the multivariate approach has been preferred to take into account spatial correlation of the EEG measurements (Nuñez, 2005). This approach yields realistic artifact-free surrogate signals. On the other hand, ocular signals are selected from real EOG measurements, which have been filtered to remove potential EEG signals. Artifact-free EEG and ocular signals are then combined in each run, as follows

$$\mathbf{x}(t) = \mathbf{EEG}(t) + \zeta \cdot \mathbf{H} \cdot \mathbf{EOG}(t), \quad (17)$$

where \mathbf{H} stands for a plausible mixing matrix, which projects the ocular noisy signal onto the EEG sensors. ζ is a varying simulation parameter, which is directly linked to the signal-to-noise ratio (SNR). In each run, for a given ζ , the multivariate Gaussian signal and the portion of EOG signal used to generate the ocular artifact are randomized. The synthetic data have been generated with a sampling rate of 250 Hz.

The hereby proposed approach, which we name *denoising by deflation* (DEFL), is compared with widely used denoising techniques based on ICA (Comon and Jutten, 2010). Two popular approaches are commonly employed for ocular artifact rejection, namely, FastICA (Makeig et al., 1996; Hyvarinen et al., 2001) and JADE (Cardoso and Souloumiac, 1993). They rely on the extraction of the most independent components according to distinct criteria. Next, semi-automatic procedures remove the components that most resemble (in the correlation sense) the ocular signals. In this study, FastICA and JADE are applied to the simulated signals $\mathbf{x}(t)$, and the components whose absolute correlations with $\mathbf{EOG}(t)$ are greater than a predefined threshold are rejected.

DEFL is implemented in a fully automatic fashion. The distribution of the moving average power $r(t)$ of the reference EOG signal is estimated to discriminate samples drawn from a Gamma distribution (resulting from a Gaussian hypothesis in the absence of ocular activity), whose estimated parameters are easily used to set an adapted threshold th .

A wavelet denoising approach is employed to remove ocular contamination from the first extracted component. The SURE policy (Donoho and Johnstone, 1995), is used to determine an adapted threshold based on the first eight wavelet decomposition levels. The wavelet decomposition is based on the Daubechies Least-Asymmetric filters, which yielded satisfactory results based on preliminary visual inspections. As mentioned before, the major advantage of wavelet denoisers for the problem of interest is that they do not dictate many assumptions on the signal smoothness or noise structure (Donoho and Johnstone, 1995).

The results of DEFL, FastICA and JADE are finally compared by quantifying the residual variance of the back-projected denoised signals with initial clean EEG signals (cf. (Makeig et al., 1996)). This yields the residual signals

$$\mathbf{e}_{\text{ICA}}(t) = \mathbf{EEG}(t) - \mathbf{x}_{\text{FastICA}}(t) \quad (18)$$

$$\mathbf{e}_{\text{JADE}}(t) = \mathbf{EEG}(t) - \mathbf{x}_{\text{JADE}}(t) \quad (19)$$

$$\mathbf{e}_{\text{DEFL}}(t) = \mathbf{EEG}(t) - \mathbf{x}_{\text{DEFL}}(t) . \quad (20)$$

The input of the algorithms consists in $n = 9$ signals, which are denoised by means of the three aforementioned methods. The length of the signals is $L = 20000$ points with a sampling rate of 250 Hz. The result is quantified by computing the normalized residual variances on each channel

$$\eta_{\text{FastICA,JADE,DEFL}} = \frac{\mathbb{V}(\mathbf{e}_{\text{FastICA,JADE,DEFL}}(t))}{\mathbb{V}(\mathbf{EEG}(t))} , \quad (21)$$

where $\mathbb{V}(\cdot)$ denotes the variance operator.

The input SNR, tuned by ζ , is swept from -50dB to 15dB in 5dB steps. Considering that a blinking artifact can typically

have an amplitude of up to 20 times stronger than the EEG and may occupy up to 20% of the signal length, the studied input SNR covers a broad range of real scenarios. Figure 3, presents the results obtained after 100 repetitions of the evaluation algorithm for each SNR. Distributions of the normalized residual variance for each method are schematically depicted by means of the median, 20 and 80 percentiles. Medians indicate that DEFL clearly outperforms results obtained using classical ICA approaches. The result is further confirmed by observing the standard deviations of the errors (the shaded bands), which show that the results obtained using DEFL are more robust than FastICA and JADE. As expected the performances of the three algorithms increase as the noise decreases. However, the proposed method is shown to clearly outperform classical ICA for a broad range of input SNRs. This effect is more significant in low SNRs, showing that the method is of particular interest for highly contaminated signals.

In order to quantify the differences between the three denoising methods, a two-step analysis of the observed performances is performed for each value of the SNR. First, an analysis of variance at fixed SNR shows that a significant difference between FastICA, JADE and DEFL exists for $-50\text{dB} \leq \text{SNR} \leq 10\text{dB}$, whereas the p-value is 0.065 for a SNR value of 15dB. Another analysis is then performed to further analyze the differences between pairwise methods. In order to correct for multiple comparisons, we used a Tukey contrast function in the pairwise t -tests computations (degree of freedom = 2). Table 1, details the results corresponding to pairwise comparisons between performances obtained by the three denoising methods. This table shows that all comparisons between DEFL and JADE or FastICA prove significant, confirming that DEFL clearly outperforms other considered methods for a broad range of SNR values. Marginally, the table also shows that the performances of FastICA and JADE cannot be ranked except for very low SNR (SNR = -50dB).

4.2. Real data

The proposed method is also evaluated using a BCI experiment dataset, recorded in the Laboratory of Brain-Computer Interfaces of Graz University of Technology ⁵ (Brunner et al., 2008). The data consists of 22 EEG channels and three EOG channels. The inter-electrode distance is about 3.5 cm. The electrode configuration is shown in Figure 4. The signals are sampled with 250 Hz and bandpass filtered between 0.5 Hz and 100 Hz. An additional 50 Hz notch filter is used to suppress power-line noise. According to the proposed method, the reference EOG channel, the normalized time-varying signal power, and the active time epoch pulse are depicted in Figure 5. For this example the sliding window length is $w=75$ samples (i.e. 300 ms), and the activation threshold is $th=0.5$. The DEFL procedure has been carried out in seven iterations. In Figure 6, a typical noisy EEG channel and the output of the first three iterations are shown. It is clearly seen that the EOG is reduced in each iteration. The original and back-projected signals after

⁵BCI competition IV, dataset 2a, subject A05 (Brunner et al., 2008)

Table 1: p -values corresponding to pairwise comparisons between FastICA (F), JADE (J) and DEFL (D). Results are only considered in cases that the analysis of variance showed a significant difference between the pairwise methods.

SNR (dB)	-50	-45	-40	-35	-30	-25	-20
F vs D	0.006	0.006	0.005	0.005	0.004	0.003	0.003
J vs D	0.003	0.004	0.003	0.004	0.004	0.003	0.002
J vs F	0.047	0.108	0.145	0.423	0.494	0.679	0.891
SNR (dB)	-15	-10	-5	0	5	10	
F vs D	0.004	0.003	0.004	0.004	0.005	0.016	
J vs D	0.003	0.003	0.003	0.003	0.005	0.015	
J vs F	0.928	0.973	0.989	0.880	0.877	0.927	

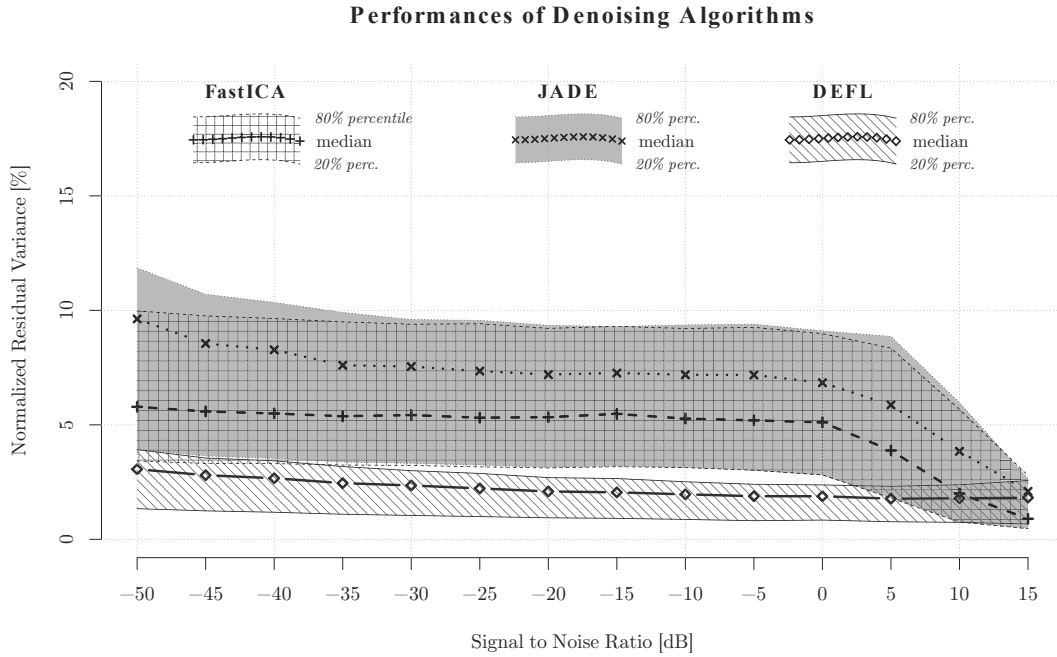


Figure 3: Distributions of Normalized Residual Variance for each three methods (FastICA, JADE and DEFL) versus signal to noise ratios tuned by ζ . Each distribution is depicted using the median, 20 and 80 percentiles.

seven iterations are depicted in Figure 7, for typical noisy channels. For comparison, the spectrum of the first channel before and after EOG removal are shown in Figure 8. By comparing the temporal and spectral performance of the algorithm, it can be concluded that although the method has filtered considerable portions of the signal energy (due to the high EOG amplitudes), but the filtering has specifically targeted the EOG portions, with minimal impact on the non-EOG segments.

The $\Delta(\cdot)$ and $\delta_i(\cdot)$ measures calculated in each iteration are listed in Table 2. Comparing the electrode configuration in Figure 4 and the results of Table 2, one can see that the frontal electrodes initially have high values of $\delta_i(\cdot)$. However, by applying the algorithm, this measure monotonically decreases from the first to the sixth iteration in all channels. In the seventh iteration the measures no longer change, showing the fact that there are no ‘significant’ EOG artifacts left and the algorithm should stop.

5. Conclusion

In this work, a novel automatic procedure was presented for removing ocular artifacts from EEG measurements without reducing the rank of the observations and with minimal influence on the temporal and frequency contents of the original EEG. The algorithm outperformed state of the art approaches based on independent component analysis. Moreover, the method is computationally efficient and has been implemented in real-time. Therefore, it is believed that due to its semi-automatic structure and low computational cost, it has broad applications in real-time EEG monitoring systems and BCI experiments, where ocular artifacts are dominant sources of noise. The hereby developed algorithm has been implemented in Matlab[®] and is online available at (Sameni, 2010).

Future works include many promising directions. Firstly, it can be shown that the optimal threshold, under Gaussian conditions can be automatically determined if a long enough period

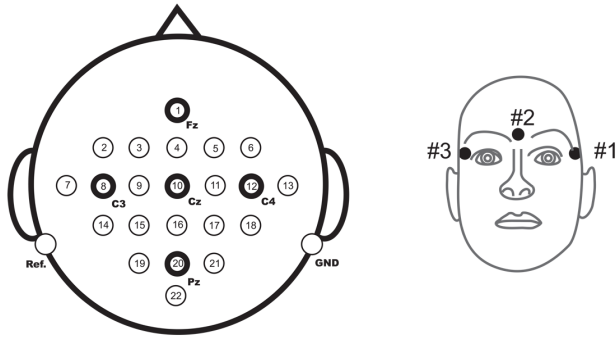


Figure 4: The EEG (left) and EOG (right) electrode configurations used in Section 4.2, adopted from (Brunner et al., 2008).

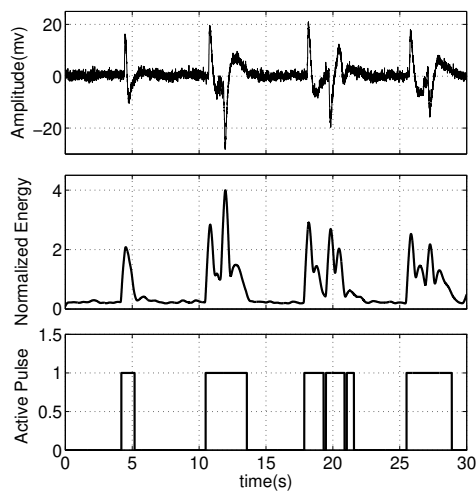


Figure 5: The reference EOG channel (top), the normalized time-varying signal power (middle), and the active time epoch pulse (bottom) for the studied dataset.

of ocular-free signals can be provided. The resulting distribution of the power in sliding windows is proved to be Gamma-distributed, yielding natural thresholds for discriminating between active and inactive ocular periods. Secondly, this article introduced the application of multiple EOG references by averaging them into a signal reference signal. It can be shown that given the automatic dimension selection procedure, the active periods of a group of channels can be determined as a whole. This procedure can indeed be seen as a robust statistical procedure that is able to generalize the classical variance ratio tests widely used in the signal processing literature.

The BCI application also requires a more thorough study, including ANOVA and pairwise t-tests for evaluating the performance of the hereby proposed techniques versus classical ICA-based methods. The sensitivity and specificity of the method should be compared with conventional techniques, using *receiver operating characteristic* (ROC) curves of various methods, over a broad real dataset.

Another promising direction is to use the robust signal-noise

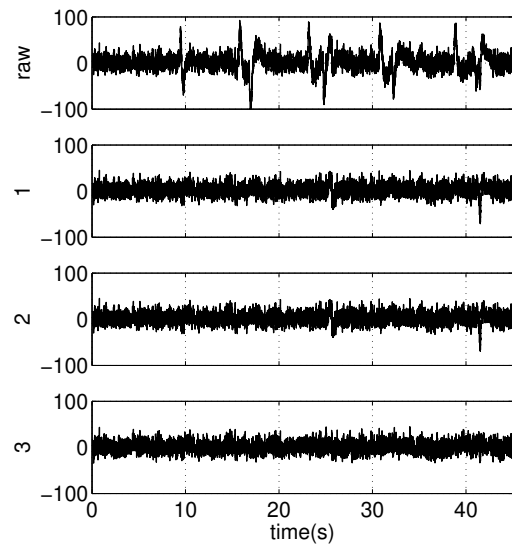


Figure 6: Noisy EEG channel (top) and the output of three successive iterations.

separation from (Nadakuditi and Edelman, 2008) to isolate active ocular periods from the EEG measurements. This approach would soften the condition that reference EOG channels are necessary to compute active periods.

References

- Amini, L., Sameni, R., Jutten, C., Hossein-Zadeh, G., Soltanian-Zadeh, H.. MR Artifact Reduction in the Simultaneous Acquisition of EEG and fMRI of Epileptic Patients. In: EUSIPCO2008 - 16th European Signal Processing Conf. Lausanne, Switzerland; 2008. .
- Anderson, C.W., Stolz, E.A., Shamsunder, S.. Multivariate autoregressive models for classification of spontaneous electroencephalographic signals during mental tasks. *IEEE Trans Biomed Eng* 1998;45(3):277–286.
- Barbati, G., Porcaro, C., Zappasodi, F., Rossini, P.M., Tecchio, F.. Optimization of an independent component analysis approach for artifact identification and removal in magnetoencephalographic signals. *Clin Neurophysiol* 2004;115(5):1220–1232. URL: <http://dx.doi.org/10.1016/j.clinph.2003.12.015>. doi:10.1016/j.clinph.2003.12.015.
- Brunner, C., Leeb, R., Müller-Putz, G.R., Schlögl, A., Pfurtscheller, G.. BCI competition 2008 – Graz dataset A. 2008. URL: http://ida.first.fraunhofer.de/projects/bci/competition_iv/desc_2a.pdf.
- Cardoso, J.F., Souloumiac, A.. Blind beamforming for non Gaussian signals. *IEE - Proceedings -F* 1993;140:362–370.
- Chan, H.L., Tsai, Y.T., Meng, L.F., Wu, T.. The removal of ocular artifacts from eeg signals using adaptive filters based on ocular source components. *Ann Biomed Eng* 2010;38(11):3489–3499. URL: <http://dx.doi.org/10.1007/s10439-010-0087-2>. doi:10.1007/s10439-010-0087-2.
- Comon, P., Jutten, C., editors. *Handbook of Blind Source Separation: Independent Component Analysis and Applications*. First edition ed. Academic Press, 2010.
- Croft, R.J., Chandler, J.S., Barry, R.J., Cooper, N.R., Clarke, A.R.. Eog correction: a comparison of four methods. *Psychophysiology* 2005;42(1):16–24. URL: <http://dx.doi.org/10.1111/j.1468-8986.2005.00264.x>. doi:10.1111/j.1468-8986.2005.00264.x.
- Delorme, A., Sejnowski, T., Makeig, S.. Enhanced detection of artifacts in EEG data using higher-order statistics and independent component analysis. *Neuroimage* 2007;34(4):1443–1449. URL: <http://dx.doi.org/10.1016/j.neuroimage.2006.11.004>. doi:10.1016/j.neuroimage.2006.11.004.

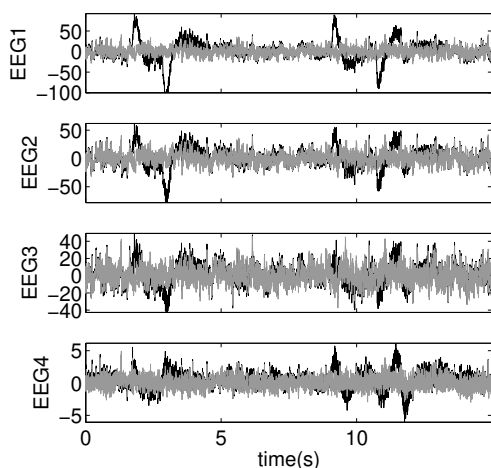


Figure 7: Four typical noisy EEG channels before (black) and after (gray) denoising.

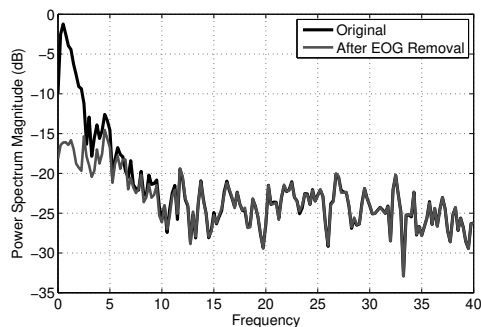


Figure 8: Spectrum of the first channel of Figure 7, before (black) and after (gray) denoising.

Donoho, D.L., Johnstone, I.M.. Adapting to unknown smoothness via wavelet shrinkage. *J Am Statist Ass* 1995;90(432):1200–1224.

Fatourechi, M., Bashashati, A., Ward, R.K., Birch, G.E.. EMG and EOG artifacts in brain computer interface systems: A survey. *Clin Neurophysiol* 2007;118(3):480–494. URL: <http://dx.doi.org/10.1016/j.clinph.2006.10.019>. doi:10.1016/j.clinph.2006.10.019.

Flexer, A., Bauer, H., Pripfl, J., Dorffner, G.. Using ICA for removal of ocular artifacts in EEG recorded from blind subjects. *Neural Netw* 2005;18(7):998–1005. URL: <http://dx.doi.org/10.1016/j.neunet.2005.03.012>. doi:10.1016/j.neunet.2005.03.012.

Gasser, T., Ziegler, P., Gattaz, W.F.. The deleterious effect of ocular artefacts on the quantitative eeg, and a remedy. *Eur Arch Psychiatry Clin Neurosci* 1992;241(6):352–356.

Gouy-Pailler, C., Sameni, R., Congedo, M., Jutten, C.. Iterative subspace decomposition for ocular artifact removal from eeg recordings. In: *Proceedings of the 8th International Conference on Independent Component Analysis and Blind Source Separation (ICA 09)*. Paraty, Brasil; 2009. p. 419–426. doi:10.1007/978-3-642-00599-2.

Gratton, G., Coles, M.G., Donchin, E.. A new method for off-line removal of ocular artifact. *Electroencephalogr Clin Neurophysiol* 1983;55(4):468–484.

He, P., Wilson, G., Russell, C.. Removal of ocular artifacts from electro-encephalogram by adaptive filtering. *Med Biol Eng Comput* 2004;42(3):407–412.

Hesse, C.W., James, C.J.. On semi-blind source separation using spatial constraints with applications in EEG analysis. *IEEE Trans Biomed Eng* 2006;53(12 Pt 1):2525–2534.

Table 2: The $\delta_i(\cdot)$ and $\Delta(\cdot)$ measures (in percents), and \hat{m}_{eff} for different iterations over real data

Iteration	0	1	2	3	4	5	6	7
$\Delta(\cdot)$	56.7	9.2	0.4	0.7	0.6	0.5	0.3	0.3
$\delta_{ch}(\cdot)$								
1	79.2	8.5	0.4	0.5	0.5	0.4	0.2	0.2
2	66.9	9.5	0.5	1.0	0.8	0.7	0.3	0.3
3	64.9	9.3	0.5	0.8	0.7	0.5	0.3	0.3
4	64.9	9.2	0.5	0.7	0.6	0.5	0.3	0.3
5	63.6	9.0	0.6	0.7	0.6	0.5	0.4	0.3
6	64.7	8.9	0.7	0.9	0.8	0.6	0.4	0.4
7	53.4	8.8	0.3	1.0	0.8	0.7	0.3	0.3
8	55.7	9.5	0.4	0.7	0.6	0.5	0.3	0.3
9	55.4	9.7	0.4	0.7	0.6	0.5	0.3	0.3
10	54.5	9.6	0.4	0.7	0.6	0.5	0.3	0.3
11	54.6	8.9	0.5	0.7	0.7	0.5	0.3	0.3
12	53.6	9.0	0.6	0.7	0.7	0.6	0.4	0.3
13	49.5	8.4	0.5	0.7	0.7	0.6	0.4	0.4
14	48.3	9.3	0.3	0.6	0.5	0.4	0.3	0.2
15	48.3	9.2	0.3	0.6	0.5	0.4	0.2	0.2
16	47.2	9.1	0.3	0.6	0.5	0.4	0.3	0.2
17	47.4	9.2	0.4	0.6	0.5	0.4	0.3	0.2
18	47.2	9.0	0.4	0.7	0.7	0.5	0.3	0.3
19	41.7	9.2	0.3	0.5	0.5	0.4	0.2	0.2
20	42.2	9.5	0.3	0.6	0.5	0.4	0.3	0.2
21	42.2	9.4	0.3	0.8	0.6	0.5	0.3	0.3
22	40.4	10.3	0.3	0.8	0.6	0.5	0.3	0.3
\hat{m}_{eff}	3	2	2	2	2	1	1	1

Hyvarinen, A., Karhunen, J., Oja, E.. *Independent component analysis*. John Wiley & Sons, 2001.

Ille, N., Berg, P., Scherg, M.. Artifact correction of the ongoing EEG using spatial filters based on artifact and brain signal topographies. *J Clin Neurophysiol* 2002;19(2):113–124.

Jung, T.P., Makeig, S., Humphries, C., Lee, T.W., McKeown, M.J., Iragui, V., Sejnowski, T.J.. Removing electroencephalographic artifacts by blind source separation. *Psychophysiology* 2000;37(2):163–178.

Koles, Z.J.. The quantitative extraction and topographic mapping of the abnormal components in the clinical EEG. *Electroencephalogr Clin Neurophysiol* 1991;79:440–447.

Lee, J.A., Verleysen, M.. *Nonlinear Dimensionality Reduction*. Springer Science, 2007.

Li, Y., Ma, Z., Lu, W., Li, Y.. Automatic removal of the eye blink artifact from EEG using an ica-based template matching approach. *Physiol Meas* 2006;27(4):425–436. URL: <http://dx.doi.org/10.1088/0967-3334/27/4/008>. doi:10.1088/0967-3334/27/4/008.

Makeig, S., Bell, A., Jung, T.P., Sejnowski, T.. Independent component analysis of electroencephalographic data. *Advances in Neural Information Processing Systems* 1996;8:145–151.

Nadakuditi, R., Edelman, A.. Sample eigenvalue based detection of high-dimensional signals in white noise using relatively few samples. *Signal Processing*, *IEEE Transactions on* 2008;56(7):2625–2638. doi:10.1109/TSP.2008.917356.

Nadakuditi, R.R., Silverstein, J.W.. Fundamental limit of sample generalized eigenvalue based detection of signals in noise using relatively few signal-bearing and noise-only samples. *IEEE Journal of Selected Topics in Signal Processing* 2010;4(3):468–480. doi:10.1109/JSTSP.2009.2038310.

Nason, G.. *Wavelet Methods in Statistics with R*. Springer, 2008.

Nuñez, P.L.. *Electric Fields of the Brain: The Neurophysics of EEG*. Oxford Univ Pr (Txt), 2005.

Romero, S., Mañanas, M.A., Barbanoj, M.J.. A comparative study of automatic techniques for ocular artifact reduction in spontaneous EEG signals based on clinical target variables: A simulation case. *Comput Biol Med* 2008;38(3):348–360. URL:

- <http://dx.doi.org/10.1016/j.combiomed.2007.12.001>.
doi:10.1016/j.combiomed.2007.12.001.
- Rousseeuw, P.J., Leroy, A.M.. Robust regression and outlier detection. Second edition ed. New York, NY, USA: John Wiley & Sons, Inc., 2003.
- Sameni, R.. The Open-Source Electrophysiological Toolbox (OSET), version 2.1; 2010. URL: <http://oset.ir>.
- Sameni, R., Jutten, C., Shamsollahi, M., Clifford, G.. Extraction of Fetal Cardiac Signals. 2010a.
- Sameni, R., Jutten, C., Shamsollahi, M.B.. Multichannel electrocardiogram decomposition using periodic component analysis. IEEE Trans Biomed Eng 2008;55(8):1935–1940. doi:10.1109/TBME.2008.919714.
- Sameni, R., Jutten, C., Shamsollahi, M.B.. A Deflation Procedure for Subspace Decomposition. IEEE Transactions on Signal Processing 2010b;58(4):2363–2374.
- Strang, G.. Linear Algebra and Its Applications. 3rd ed. Brooks/Cole, 1988.
- Thulasidas, M., Guan, C., Ranganatha, S., Wu, J., Zhu, X., Xu, W.. Effect of ocular artifact removal in brain computer interface accuracy. In: Conf. Proc. IEEE. Eng. Med. Biol. Soc. volume 6; 2004. p. 4385–4388. URL: <http://dx.doi.org/10.1109/IEMBS.2004.1404220>. doi:10.1109/IEMBS.2004.1404220.
- van Trees, H.. Detection, Estimation, and Modulation Theory, Part IV, Optimum Array Processing. John Wiley & Sons, 2002.